ACS APPLIED MATERIALS & INTERFACES

Research Article

www.acsami.org

Solvent-Controlled Synthesis of NiO–CoO/Carbon Fiber Nanobrushes with Different Densities and Their Excellent Properties for Lithium Ion Storage

Yuehua Wei,[†] Feilong Yan,[†] Xuan Tang,[†] Yazi Luo,[†] Ming Zhang,*[,†] Weifeng Wei,[‡] and Libao Chen*[,‡]

[†]Key Laboratory for Micro-Nano Optoelectronic Devices of Ministry of Education, School of Physics and Electronics, State Key Laboratory for Chemo/Biosensing and Chemometrics, Hunan University, Changsha, 410082, People's Republic of China

[‡]State Key Laboratory for Power Metallurgy, Central South University, Changsha, 410083, People's Republic of China

Supporting Information

ABSTRACT: NiO–CoO nanoneedles are grown on carbon fibers by a solvothermal strategy to form nanobrushes. The density of nanobrushes can be easily controlled by altering the solvents. The synthesis mechanism of NiO–CoO/carbon fiber nanobrushes is investigated by the time-dependent experiments in detail. As anodes for lithium ion batteries, the NiO–CoO/carbon fiber nanobrushes synthesized in ethanol show excellent properties with a discharge capacity of 801 mA h g^{-1} after 200 cycles at a current density of 200 mA g^{-1}. The improvement can be ascribed to the carbon fibers as the highway for electrons and the interspace between NiO–CoO nanoneedles to accommodate the volume change and maintain the structural stability.

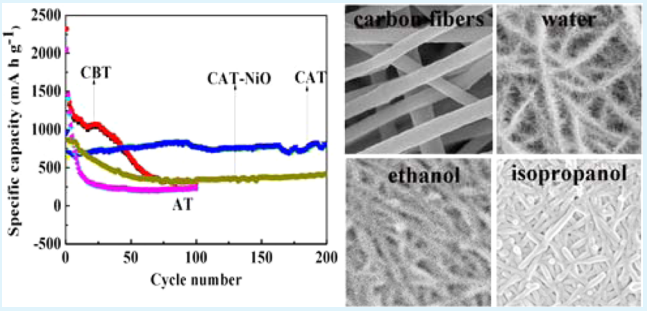

KEYWORDS: *NiO–CoO/carbon fiber nanobrushes, NiO–CoO nanoneedles, NiO/carbon fiber nanobrushes, carbon fibers, solvents, lithium ion batteries*

INTRODUCTION

In order to reduce the rapid depletion of fossil-fuel and environmental pollution over the past few years, much effort has been concerned with developing energy conversion–storage devices.[1−3] Because of their high working voltages, considerable capacities, and nontoxicity, lithium ion batteries (LIBs) have been considered as one of the most promising candidates.[1,4−6] Currently, the most commercially popular anode is graphite, but new materials are needed to meet the demand of LIBs with higher energy density and power density. Moreover, compared to two-dimensional (2D) structures, three-dimensional (3D) structures with large surface areas, better permeabilities, and more active sites exhibited ultrahigh capacity, excellent cycling performance, and good rate discharging/charging stability.[7−9] Many studies have been focused on the nanostructured metal oxides (including binary and mixed oxides) as alternative anode materials for LIBs because of the high theoretical capacities.[10−13] Among them, NiO and CoO stand out as the most promising materials owing to their high theoretical capacities (716 and 718 mA h g^{-1}).[14−18] As reported in the previous studies, the incorporation of metals (such as Au, Ni, etc.) could significantly enhance the electrochemical performance of transition metal oxides because of the catalytic effect of the metal particles generated in the discharge process. Therefore, it is interesting to study NiO–CoO nanocomposites with the catalytic effect of the metal phase.[19−22] Besides, it is of great significance to construct NiO–CoO nanocomposites with a hierarchical structure. Another issue is that the low electronic conductivity and low stability of NiO and CoO during the redox reaction have hindered their practical applications in LIBs.

To overcome those obstacles, various effective strategies have been developed to boost the reversible capacity, rate capacity, and cycle life of NiO and CoO based materials. For example, materials at the nanoscale, such as nanowires, nanotubes, and hollow nanospheres, have been successfully developed.[23−26] Although nanosized materials can improve their electrochemical performances to some extent, the limited cycle life and inferior rate capability are restricted due to their poor electrical conductivity.[18,23,27,28] Because of the high conductivity and good stability, many conductive carbon materials (such as carbon nanotubes (CNTs), graphene, and so on) as electrical highways and mechanical backbones have been widely studied as electrode materials in lithium ion batteries.[29] Hence, hybridization nanostuctural materials with highly conductive carbon materials, which helps the faster electron transport during lithiation/delithiation processes, has been extensively designed for the enhanced cycling performance.[17,28,30,31] Due

Received: May 12, 2015
Accepted: September 15, 2015
Published: September 15, 2015

DOI: 10.1021/acsami.5b07233
ACS Appl. Mater. Interfaces 2015, 7, 21703−21711

to their outstanding electrical properties, including high chemical stability, high aspect ratio, strong mechanical strength, and high activated surface area, CNTs can rapidly upgrade the performance of nanostructured transition metal oxides.[32,33] However, the main weakness of CNTs is the low efficiency and low loading density of transition metal oxides. Because of the outstanding electrical conductivity and superior mechanical flexibility, graphene is a well-suited candidate for high-performance lithium ion battery electrodes.[29,34] Nevertheless, layered stacking graphene resulting from the huge surface area and strong $\pi-\pi$ interactions between graphene layers has a much smaller surface area and the conductivity of graphene decreases when more defects are introduced.[35] Carbon-coated materials, as one of the most common methods to increase the properties of transition metal oxides, could not solve the large volume expansion and agglomeration of the active metal oxide nanostructures during the charge−discharge processes because of the restricted space between carbon and metal oxides. Carbon fibers, consisting of amorphous carbon and a network of nanosized carbon fibers compared with carbon cloth, have large surface area, high porosity, good electric conductivity, and excellent chemical stability in lithium ion batteries, which could significantly enhance the cycle life and rate capability of the nanostructured materials by shortening the distance of electron transport.[36−38] Inspired by hybridization of nanosized materials with carbon cloth, we combined the metal oxides with carbon fibers to enhance the Li storage properties during the repeated charge/discharge processes.

Herein, we develop a strategy for the fabrication of NiO−CoO nanoneedles on carbon fiber substrates to form a 3D NiO−CoO/carbon fiber nanobrush structure, exhibiting excellent cycling performance and good rate capability. The following can be highlighted for this fabrication: (1) The NiO−CoO nanocomposite with higher synergistic electrocatalytic behavior and the original advantages of the two metal oxides possessed excellently improved electrochemical performance than the single metal oxide due to the metallic nanoparticles generated by transition metal oxides in the discharge process, which could be catalyzed by the decomposition of the solid−electrolyte layer (SEI) in the charge process.[20,39] (2) Synthesis of 3D NiO−CoO/carbon fiber nanobrushes involved three steps: the preparation of carbon fibers with electrospinning, hydrothermal epitaxial growth of porous 3D NiO−CoO/carbon fiber nanobrush precursor, and subsequent heat treatment process.[8] (3) As far as we know, it is a new strategy to use carbon fibers by electrospinning as the backbones to prepare NiO−CoO/carbon fiber nanobrushes. The resulting brushlike nanostructure presents excellent chemical stability in a great diversity of liquid electrolyte in contrast to previous morphologies, resulting in better cycling stability and durable rate behavior. (4) The NiO−CoO nanoneedles which were strongly supported on the carbon fiber substrates can significantly enhance the rate capability and cycling stability of the active materials by shortening the distance of electron transport.

EXPERIMENTAL SECTION

Preparation of Carbon Fibers. All reagents were of analytical grade and used without any further purification. Polyacrylonitrile (PAN, M_w = 150 000, Sigma-Aldrich Co., Ltd.) was first dissolved in *N*,*N*-dimethylformide under magnetic stirring to form a homogeneous viscous solution at 50 °C temperature for no less than 6 h. Then the precursor solution was shifted into a 5 mL syringe with a stainless steel needle (with an inner diameter of 0.71 mm). A syringe pump was used to control the flow rate of the precursor solution to about 0.2 mL h^{-1}. The resultant fibers were collected on a piece of aluminum foil, which was vertically positioned about 15 cm from the needle point. The high voltage dc power supplied to obtain a voltage of 6−10 kV was used to control the needle point. The materials were then dried in a vacuum at 60 °C. After this, the preoxidized nanofibers were obtained by annealing the as-spun fibers at 230 °C for 6 h in air. Finally, the resulting fibers were treated at 600 °C in Ar for 2 h in order to carbonize the PAN.

Preparation of NiO−CoO Nanoneedles on the Carbon Fibers. First, self-supported NiO−CoO nanoneedles were prepared by a facile hydrothermal synthesis method. In a typical procedure, 0.291 g of $Co(NO_3)_2{\cdot}6H_2O$, 0.566 g of $Ni(NO_3)_2{\cdot}6H_2O$, and 0.96 g of urea were dissolved in 17 mL of deionized (DI) water and 3 mL of ethanol. Subsequently, the above mixed solution stirred for 20 min became transparent pink. Then the solution was transferred into a 50 mL Teflon-lined stainless steel autoclave. A 0.3 mg sample of carbon fibers was then immersed into the above solution followed by heating of the solution to 120 °C in an oven for 12 h and cooling to room temperature. The as-synthesized carbon fibers were then taken off and rinsed with DI water and ethanol and dried at 80 °C in air overnight. Finally, the obtained productions were annealed at 300 °C in Ar for 2 h to gain NiO−CoO nanoneedles on the carbon fibers. Samples using different solvents were also synthesized under the same experimental conditions except replacing 3 mL absolute ethanol with water and isopropanol.

Electrode Preparation and Electrochemical Characterization. The morphologies and sizes of the samples were determined by a field emission gun scanning electron microscope (FESEM, Hitachi S-4800) at an accelerating voltage of 5 kV. The crystalline phases of the synthesized samples were carried out by X-ray diffraction (XRD) on a Rigaku Desktop X-ray diffractometer using Cu Kα (λ = 1.5418 Å) radiation. The structures of the samples were also studied using transmission electron microscopy (TEM, JEOL JEM-2100F microscope). XPS data was collected with X-ray photoelectron spectroscopy. The thermal gravimetric analysis was recorded on a thermogravimetric analyzer (TGA, PerkinElmer, Diamond TG/DTA) in air with a heating rate of 3.5 °C min^{-1}. The samples were heated from room temperature to 800 °C. The electrochemical impedance spectroscopy (EIS) measurements were performed on a CHI660e electrochemical workstation at frequencies ranging from 0.01 Hz to 1 MHz. The working electrodes of NiO−CoO nanoneedles on the carbon fibers/acetylene black/polyvinylidene difluoride (PVDF) in a weight ratio of 8:1:1 mixed *N*-methylpyrrolidinone (NMP) were fabricated with a copper strip as the current collector. The obtained specific capacities were calculated by the mass of whole materials (both NiO−CoO and carbon fibers), which was 0.82 mg/cm^2.

RESULTS AND DISCUSSION

The morphologies of the different phase products were examined with scanning electron microscopy (SEM). Figure 1 presents images of carbon fibers and different NiO−CoO/carbon fiber nanobrushes, which shows the morphological changes of nanostructures with different solvents. The carbon fibers (Figure 1a), synthesized through an electrospinning method with diameters of 300−400 nm, intrinsically show interconnected structure and continuous framework. After the facile hydrothermal process, the carbon fibers were successfully covered with disordered NiO−CoO nanoneedles by using water as solvent, as shown in Figure 1b. The solvent was mixed with a little absolute ethanol, and the morphology of these brushlike NiO−CoO/carbon fiber composites, which were strongly supported on the carbon fiber substrates, is presented in Figure 1c. Moreover, Figure 1d depicts a typical SEM image of the as-made samples with higher density when absolute ethanol was substituted with isopropanol. The FESEM images of the as-formed products using the solvent of water and a little

DOI: 10.1021/acsami.5b07233
ACS Appl. Mater. Interfaces 2015, 7, 21703−21711

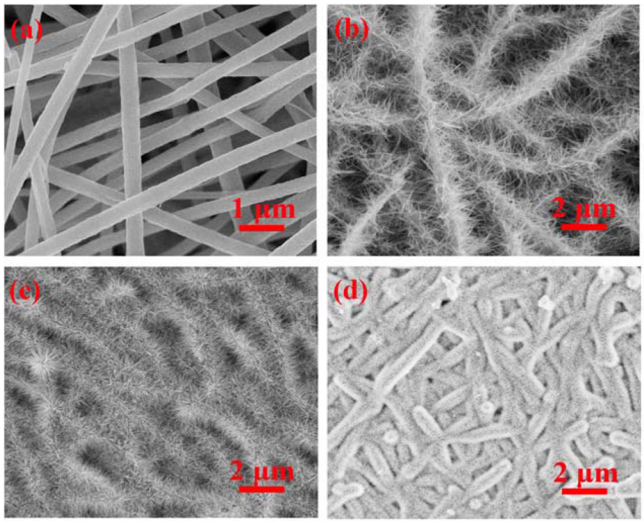

Figure 1. SEM images of (a) pure carbon fibers and samples synthesized in different solvents: (b) water; (c) absolute ethanol; (d) isopropanol.

isopropanol are displayed in Figure S1, which can clearly show the oriented NiO−CoO nanoneedles strongly supported on the carbon fibers. Those results show the great effect of solvent on the nucleation and growth of NiO−CoO nanoneedles. A possible reason may be that ethanol and isopropanol can reduce the surface tension and alter the polarity and coordination ability of the solvent so that the nucleation and growth of nanoneedles are strong affected. The small nanoneedle diameter allows for the accommodation of volume changes without pulverization that can occur in bulk or micrometer-sized materials, which is consistent with previous studies.[40] Therefore, the density of the nanoneedle is very important for the electrochemical performance. In this paper, little ethanol was used as an additive for hydrothermal process to control the density of NiO−CoO nanoneedles. We could also obtain the NiO−CoO nanospheres without carbon fibers, as seen in Figure S3.

In our synthesis strategy, there are three steps including electrospinning, hydrothermal treatment, and subsequent calcination process in Ar. Figure 2 shows the general morphologies for carbon fibers and NiO−CoO/carbon fiber nanobrushes. First, continuous framework and interconnected carbon fibers were synthesized through the electrospinning method, as shown in Figure 2a. Then the metal oxide/carbon fiber composites as the precursor were obtained by a facile hydrothermal method, which used the solvents of water, absolute ethanol, and isopropanol, respectively. After a simple nonequilibrium heat treatment process, the metal oxide/carbon fiber composites could be easily converted to NiO−CoO/carbon fiber nanobrushes which still keep the framework and

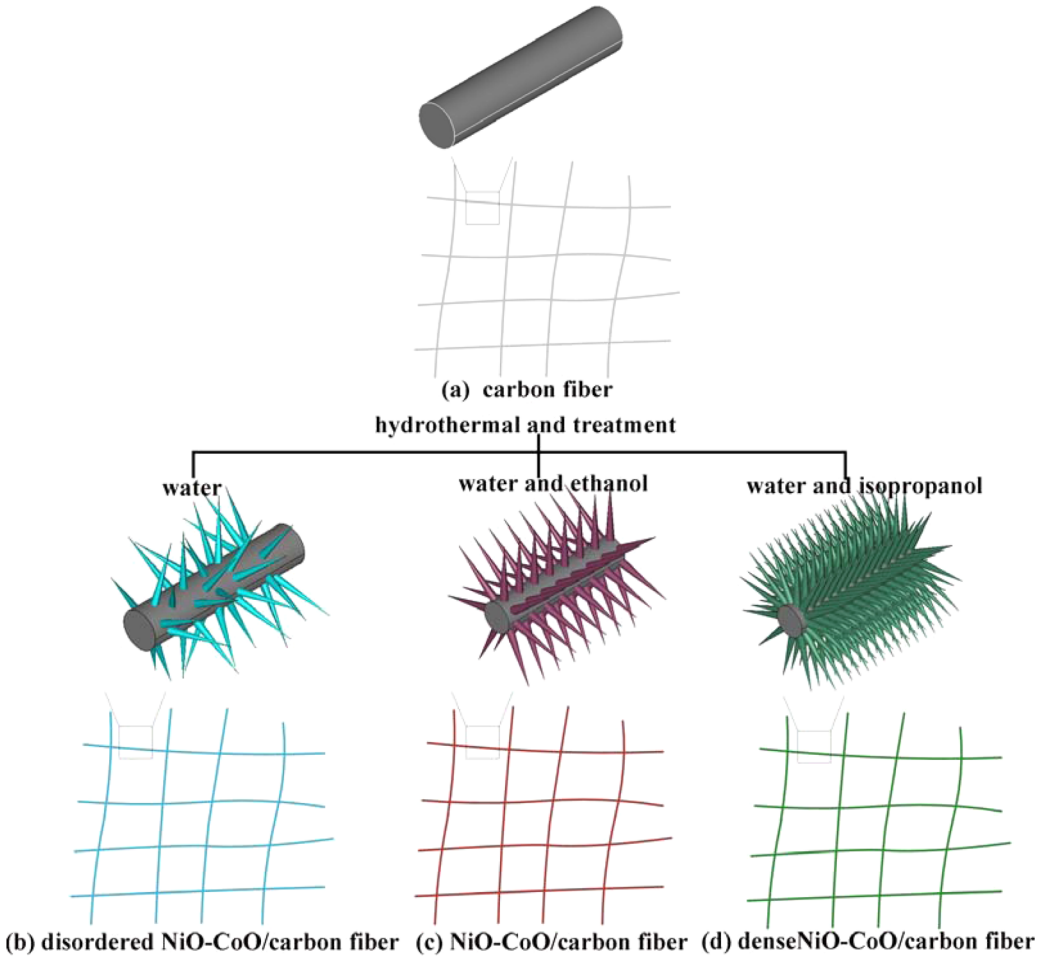

Figure 2. Schematic illustrations of (a) carbon fibers, (b) disordered NiO−CoO/carbon fiber nanobrushes, (c) NiO−CoO/carbon fiber nanobrushes, and (d) dense NiO−CoO/carbon fiber nanobrushes.

DOI: 10.1021/acsami.5b07233
ACS Appl. Mater. Interfaces 2015, 7, 21703−21711

interconnected structure of the carbon fiber substrates, as shown in Figure 2b–d. Meanwhile, we can also clearly see NiO–CoO nanoneedles with high density grown almost vertically on carbon fibers to form a large-scale conformal coating.

The time-dependent experiments were also investigated to show the synthesis mechanism of the hydrothermal reaction preparing NiO–CoO/carbon fiber nanobrushes. The corresponding SEM images of morphological evolutions are applied to trace the growth process, as presented in Figure 3 while

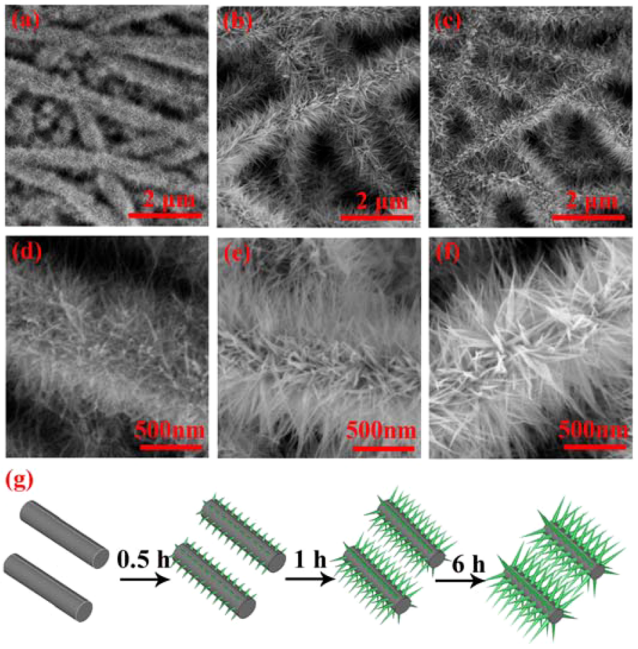

Figure 3. SEM images of NiO–CoO/carbon fiber nanobrushes at different reaction times: (a, d) 0.5 h; (b, e) 1 h; (c, f) 6 h. (g) Synthesis mechanism of the NiO–CoO/carbon fiber nanobrushes.

keeping other experimental conditions the same, except for reaction time. When we controlled the reaction time at 0.5 h, the nanobrushes were just sprouted, as shown in Figure 3a,d. As the reaction time added up to 1 h, it could be clearly seen that the NiO–CoO nanoneedles were gradually grown. Figure 3b,e reveals the relevant results. After hydrothermal treatment for 6 h, the morphology of NiO–CoO/carbon fiber nanobrushes is presented in Figure 3c,f. From the SEM images observed for different times, the synthesis mechanism of the NiO–CoO/carbon fiber nanobrushes is proposed, as shown in Figure 3g. Before reactions, the surface of carbon fibers was smooth. After 0.5 h, a great deal of small NiO–CoO nanoneedles which were derived from Ni and Co precursors were observed in the SEM images of Figure 3a,d. With the reaction time increased, the crystal growth stage then transferred to a kinetically controlled process and the nanobrushes were grown from the small nanoneedles.[41,42] Owing to the gradual reduction of the reactant concentration, the crystal growth continued in progress, leading to the gradual growth of nanobrushes, as shown in Figure 3c,f.

The detailed structural features of NiO–CoO/carbon fiber nanobrushes were further characterized by FESEM. In Figure 4a, NiO–CoO nanoneedles strongly supported on carbon fibers can be seen. In Figure 4b, the panoramic FESEM image reveals a single carbon fiber composed of many uniform

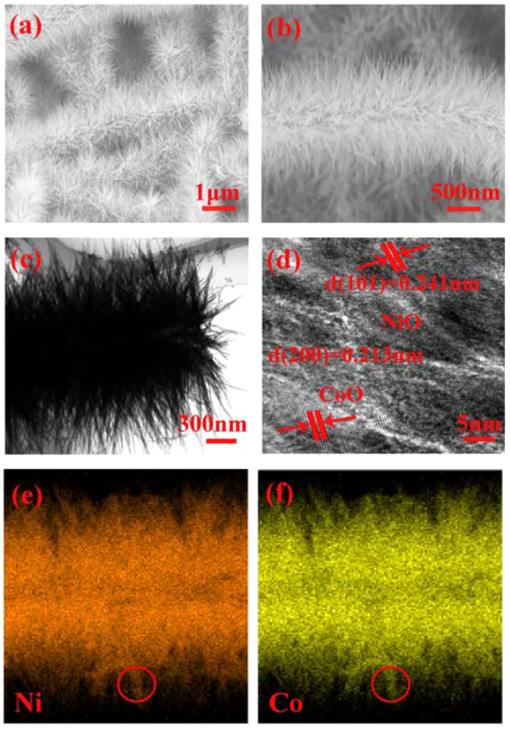

Figure 4. (a, b) FESEM images of NiO–CoO/carbon fiber nanobrushes prepared in a solution of water and ethanol at different magnifications. (c, d) TEM and HRTEM images of carbon fibers covered with NiO–CoO nanoneedles. (e, f) Element mappings of Ni and Co, respectively.

nanoneedles with diameters of 20–30 nm. The microstructural nature and morphology of these NiO–CoO/carbon fiber nanobrushes were further elucidated using transmission electron microscopy (TEM). As shown in Figure 4c, NiO–CoO nanoneedles with high density were almost radially grown on the carbon fiber cores to form NiO–CoO/carbon fiber nanobrushes, which were in good agreement with the results obtained from the SEM observation. The high resolution TEM (HRTEM) image presented in Figure 4d reveals the (200) plane of CoO and (101) plane of NiO, corresponding to three sets of lattice fringes with interplane spacings of 0.213 and 0.241 nm, respectively. From the element mappings, it is clearly observed that the elements of Ni and Co are uniformly distributed in the nanobrushes. In the sections marked with red, there are many Ni elements while the element of Co is also distributed in the same section. Therefore, it is difficult to know the sizes of the NiO and CoO.

In order to further confirm the crystallographic structure of the as-synthesized products, X-ray diffraction (XRD) is also conducted to detect the NiO–CoO nanoneedles without carbon fibers and the corresponding results are presented in Figure 5a. After the themolysis of the nickel cobalt precursors, all of the products could be successfully indexed as NiO–CoO crystalline structure (JCPDS Card Nos. 44-1159 and 70-2855). Moreover, it is found that no residues or contaminants have been detected, indicating the high purity of the as-synthesized samples. No peaks which can be indexed to carbon were found in the XRD pattern, showing the low crystallinity and degree of graphitization of PAN-based carbon obtained at about 600 °C.[43] In the Supporting Information (Figure S7), the phase and morphology of the as-prepared sample before the heat

DOI: 10.1021/acsami.5b07233
ACS Appl. Mater. Interfaces 2015, 7, 21703–21711

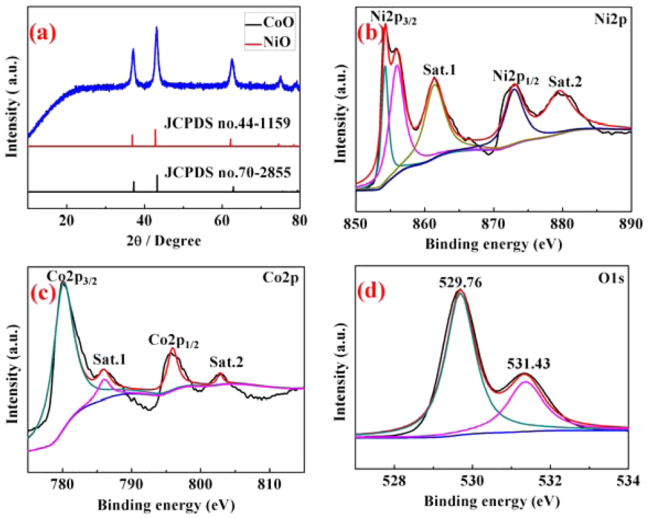

Figure 5. (a) Typical XRD patterns and JCPDS information for NiO (44-1159) and CoO (70-2855). (b–d) High-resolution XPS spectra of (b) Ni, (c) Co, and (d) O in NiO–CoO/carbon fiber nanobrushes.

treatment were obtained. The XRD pattern cannot be indexed to a single phase, suggesting complicated phase compositions.

Because of the similar XRD patterns of NiO and CoO, further evidence for the elemental composition and the oxidation station of the as-synthesized products was obtained by X-ray photoelectron (XPS) measurements, as shown in Figure 5b–d. It can be observed from Figure 5b that there are two shake-up satellites (indicated as "Sat."), which are in accordance with previous reports.[44,45] Another two typical peaks, located at 854.2 and 872.9 eV in the high-resolution Ni 2p spectrum, correspond to the Ni $2p_{3/2}$ and Ni $2p_{1/2}$ spin–orbit levels of NiO, respectively.[46,47] An additional peak feature besides those at 855.9 eV with a small shoulder is presumably due to the small existence of Ni_2O_3 phase in the film.[43] According to previous reports, the two typical peaks of the Co 2p spectrum, centered at 780.1 and 795.9 eV, are indexed to the Co $2p_{3/2}$ and Co $2p_{1/2}$ spin–orbit peaks of CoO.[16,18,48−51] The fitting peak of O 1s at the binding energy (BE) of 529.7 eV is well matched with the typical metal–oxygen bond of Ni–O/C–O–Ni/Co–O/C–O–Co, while the binding energy peak at 531.4 eV corresponds to the H–O bonds of the surface hydroxyl groups.[45] Further evidence of the purity of the materials show that no other peaks besides those for Ni, Co, O, and C could be seen in the wide-survey XPS spectrum, as shown in the Supporting Information (Figure S5).[52]

The thermal behavior and mass ratio of the NiO–CoO/carbon fiber nanobrushes were further determined with the TGA measurement in air, as shown in Figure 6a. A small weight loss was observed between 100 and 320 °C, which can be ascribed to the water evaporation. The composites made with 20 wt % carbon fibers show an obvious weight loss at about 320 °C due to carbon combustion. After 800 °C, the final products were further characterized by XRD to determine NiO and CoO, as shown in Figure 6b. The NiO–CoO/carbon fiber nanobrushes show a total weight loss of 25.5%, while the weight fraction of NiO–CoO in composites is calculated to be 74.5%.

To better understand the electrochemical behavior of the electrodes, a cyclic voltammetry (CV) test (Figure 7a) was carried out at a scan rate of 0.1 mV s^{-1} for a voltage of 0.01–3 V. As can be seen, there are well-defined sharp oxidation peaks at 1.64/2.25 V, derived from the oxidation of Ni^0 to Ni^{2+} and Co^0 to Co^{2+}.[49,53,54] In addition, a single primary reduction peak at approximately 0.48 V in the first cathodic scan was observed, corresponding to the initial reduction of NiO–CoO to metallic Ni–Co, the irreversible formation of a solid–electrolyte interface (SEI) layer, and the decomposition of electrolyte. In the subsequent cycles, there is no significant change in the potentials of the oxidation peaks at 1.64 and 2.25 V, while the reduction peak becomes weak and shifts to 1.0 V.[3,16,18]

Subsequently, the electrochemical properties of these NiO–CoO/carbon fiber nanobrushes as anode materials for LIBs are investigated by galvanostatic charge–discharge measurements. The representative charge–discharge voltage profiles between 0.01 and 3.0 V for the first, second, and 200th cycles at a current rate of 200 mA g^{-1} are shown in Figure 7b. The initial discharge capacity of these NiO–CoO/carbon fiber nanobrushes is about 961.53 mA h g^{-1}, whereas the corresponding charge capacity is around 692 mA h g^{-1}, indicating a irreversible capacity loss of about 38%. This agrees well with NiO and CoO based electrode materials that the reduction peaks are present in the first cathodic scan but disappear afterward. The long stable voltage stage at 1.0 V in the first discharge is due to the complex phase transformation of CoO–NiO to Co–Ni and the SEI formation, which are a good match with the CV test. In the charge process, two plateaus around 1.6 and 2.2 V can be seen, which are in common with the anode peaks of the CV result.

Figure 7c shows the cycling performance of the NiO–CoO/carbon fiber nanobrush electrodes before and after heat

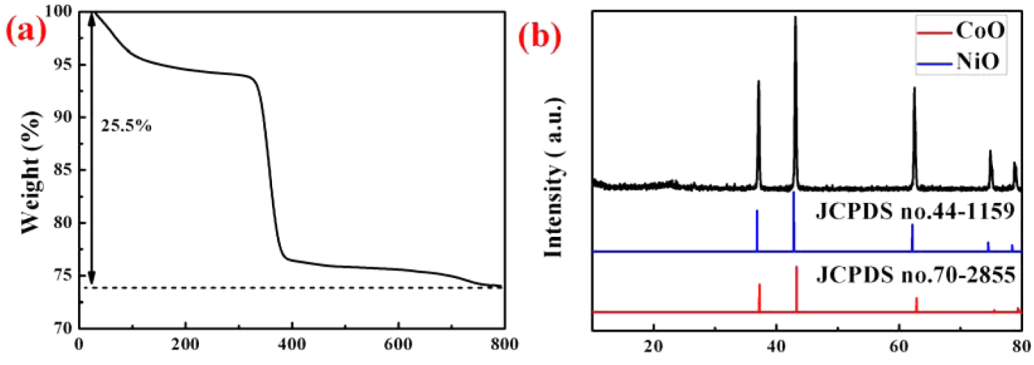

Figure 6. (a) TGA curve of NiO–CoO/carbon fiber nanobrushes in air with a heating rate of 3.5 °C min^{-1}. (b) Typical XRD patterns of NiO–CoO/carbon fiber after 800 °C and JCPDS information for NiO (44-1159) and CoO (70-2855).

DOI: 10.1021/acsami.5b07233
ACS Appl. Mater. Interfaces 2015, 7, 21703–21711

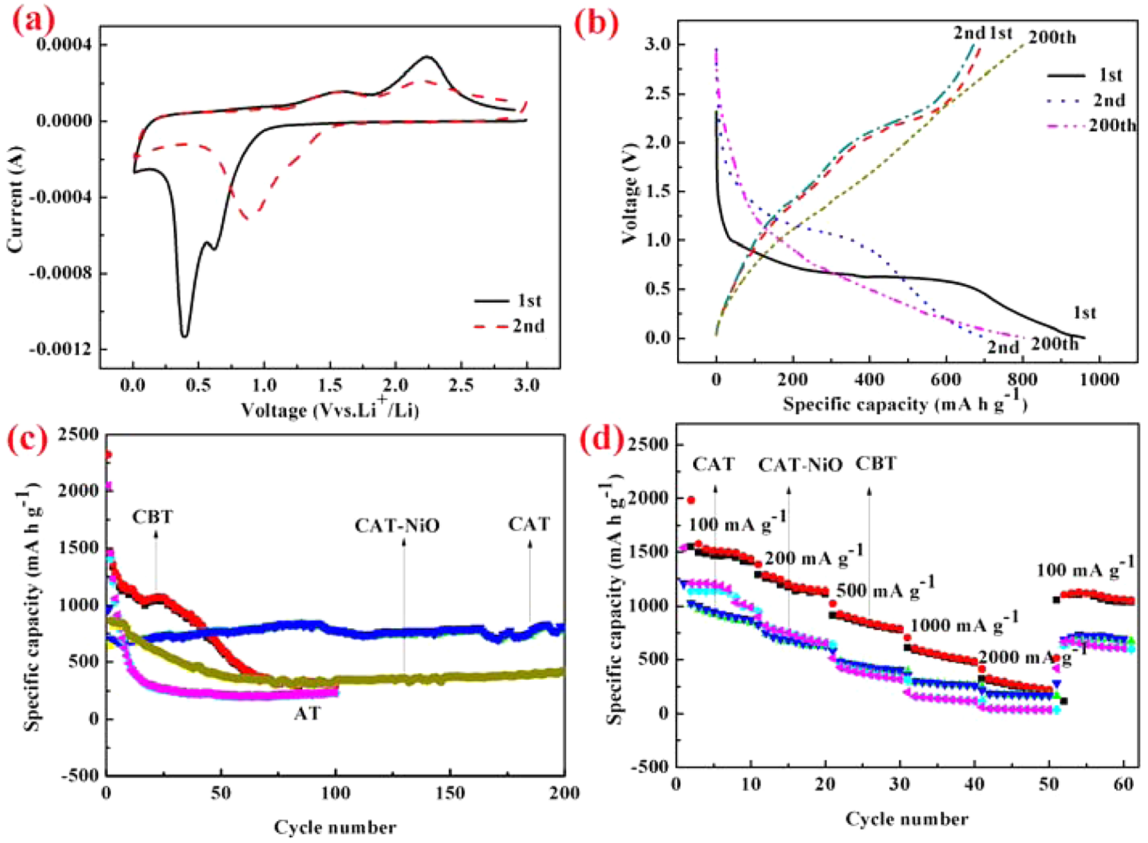

Figure 7. (a) CV curves of NiO−CoO/carbon fiber nanobrushes between 0.01 and 3.0 V at the sweep speed of 0.1 mv/s. (b) Charge−discharge curves of NiO−CoO/carbon fiber nanobrushes at a current density of 200 mA g^{-1}. (c) Cycling performances of NiO−CoO/carbon fiber nanobrushes before and after heat treatment (CBT and CAT), NiO−CoO nanosphere electrode (AT),and NiO/carbon fiber nanobrushes (CAT-NiO) at 200 mA g^{-1}, respectively. (d) Rate-capability properties of NiO−CoO/carbon fiber nanobrushes before and after heat treatment (CBT and CAT) and NiO/carbon fiber nanobrushes (CAT-NiO at different current densities).

treament, NiO−CoO nanosphere electrode and NiO/carbon fiber nanobrush electrodes were tested at the current density of 200 mA g^{-1}. For these NiO−CoO/carbon fiber nanobrush electrodes after treatment, a capacity of 961.53 mA h g^{-1} was delivered in the first lithiation and the irreversible capacity of 269 mA h g^{-1} was mainly ascribed to the formation of SEI film.[55] Clearly, the electrode can still deliver a stable capacity of 801.8 mA h g^{-1}after 200 cycles, demonstrating excellent cycling stability. The increasing capacity in the first 20 cycles may be due to an activation process which is caused by the enlarged surface area after a nanosize effect. Although these brushlike nanohybrid electrodes except treatment delivered a capacity of 2320.7 mA h g^{-1} in the first cycles, the capacity decreased after 30 cycles, resulting from the deterioration of the structure. After 100 cycles, only 440 mA h g^{-1} is retained under the same conditions. For comparison, bare NiO−CoO nanospheres were also tested under the same electrochemical conditions to further demonstrate the effect of the carbon fibers. However, the capacities of the bare NiO−CoO nanospheres and NiO/carbon fiber nanobrush electrodes dropped rapidly from those of the initial several cycles and carbon fibers can deliver a capacity of only 370 and 320 mA h g^{-1}. Here, the enhanced Li^+ storage property and improvement of high cyclic performance for these NiO−CoO/carbon fiber nanobrushes can be mainly attributed to the large surface area, high porosity, and good electric conductivity of carbon fibers and the advantage of NiO−CoO nanoneedles (shown in Figure 8). This nanobrush structure shortens the diffusion path of Li^+ in the nanomaterials.[8] The open space between neighboring nanoneedles, which provides ideal conditions for facile diffusion of the electrolyte during the electrochemical process, allows for the quick

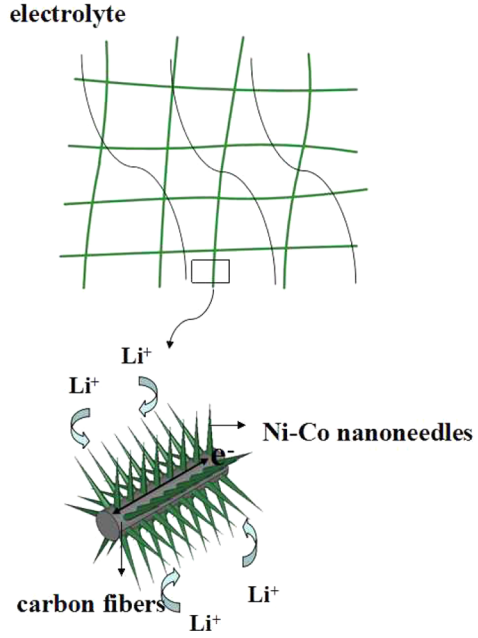

Figure 8. Schematic of advantages of NiO−CoO nanoneedles on carbon fibers.

DOI: 10.1021/acsami.5b07233
ACS Appl. Mater. Interfaces 2015, 7, 21703−21711

lithiation and delithiation of Li^+ and accommodation of the strain aroused by the volume change during charge and discharge processes, and the carbon fibers can provide numerous fast electronic transfer channels to improve the electrochemical performance.[41,56] Moreover, nickel has been reported as a good catalyst for the decomposition of Li_2O in a previous study.[39] As reported in previous studies, the incorporation of metals (such as Au, Ni, etc.) could significantly enhance the electrochemical performance of transition metal oxides because of the catalytic effect of the metal particles generated in the discharge process. The catalytic effect of Ni particles on the decomposition of Li_2O can reduce the initial irreversible capacity.

Apart from the excellent stable cycle capability, the rate capacity is another outstanding feature of this electrode. To further evaluate the rate capability, the NiO−CoO/carbon fiber nanobrush electrodes before and after treatment and the NiO/carbon fiber nanobrush electrodes were cycled from current densities of 100 to 2000 mA g^{-1} for 10 cycles at each current density, as shown in Figure 7d. Remarkably, the capacities of the NiO−CoO/carbon fiber nanobrush electrode after treatment keep steadier than those of the electrode without treatment. More importantly, this situation is obvious when the current density is increased. In addition, when the current density is brought back down to 100 mA g^{-1} after such high current cycling, the capacity of these NiO−CoO/carbon fiber nanobrushes swiftly recovers and the Coulombic efficiency is nearly 100%. Similar to the cycling performance, the NiO−CoO/carbon fiber nanobrush electrode without treatment and NiO/carbon fiber nanobrush electrodes still present inferior rate capabilities compared with that of the electrode after treatment. The impedance spectra of these NiO−CoO/carbon fiber nanobrushes and NiO/carbon fiber nanobrushes after 200 cycles are displayed in Figure S8. The smaller semicircular diameter of NiO−CoO/carbon fiber nanobrushes implied a lower charge transfer resistance than NiO/carbon fiber nanobrushes and may be the reason resulting in the enhanced cycling performance.[60] Based on the equivalent circuit (inset of Figure S8) for fitting, the charge transfer resistance (R_{ct}) for NiO−CoO/carbon fiber nanobrushes and NiO/carbon fiber nanobrushes are 79.29 and 175.3 Ω. This may be attributed to the high conductivity and the catalytic effect of Ni^0 generated in the discharge process. Compared to the previous studies, it could be observed that the NiO−CoO/carbon fiber nanobrushes also delivered a relatively high specific capacity and cyclic stability, as shown in Table 1.

Table 1. Specific Capacities and Cyclic Properties of NiO−CoO/Carbon Fiber as Anodes for LIBs

material	current density (mA h g^{-1})	reversible capacity (mA h g^{-1})	ref
Co-doped NiO	100	589.5 (50th)	57
NiO/Co−P nanocomposite	100	540 (50th)	58
nanosheet-based NiO nanosphere	50	100 (30th)	59
NiO film	100	687 (50th)	45
CoO−NiO−C	100	268 (60th)	39
$CoNiO_2$ hierarchical structure	100	449.3 (50th)	3
NiO−CoO/carbon fiber nanobrushes	200	801 (200th)	this study

CONCLUSIONS

In summary, NiO−CoO nanoneedles directly grown on carbon fibers were successfully prepared through electrospinning, hydrothermal method, and following a simple thermal treatment. By changing solvents and reaction time, the structure of a nanobrush can be easily regulated. For LIB application, it presented a capacity of 961.53 mA h g^{-1} at the current density of 200 mA g^{-1}. Even after 200 cycles, it still delivered the capacity of 801.8 mA h g^{-1}, and showed good cycling stability and rate capability. Until now, carbon fibers were rarely used, prepared by electrospinning as conductive substrates to support NiO−CoO nanoneedles. The intertconnected structures and continuous framework lead to the excellent electrochemical performance. Furthermore, the strategy of covering NiO−CoO nanoneedles on carbon fibers to enhance the cycling stability and rate capability could be extended to other materials, such as MnO_2, MoS_2, and Fe_2O_3, which presents potential applications in large-scale energy storage systems.

ASSOCIATED CONTENT

Supporting Information

The Supporting Information is available free of charge on the ACS Publications website at DOI: 10.1021/acsami.5b07233.

FESEM images of as-formed products using the solvents of water and little isopropanol; SEM and FESEM images of NiO/carbon fiber nanobrushes, NiO−CoO nanospheres, carbon fibers, CoO, and as-prepared sample before heat treatment; XPS spectra of NiO−CoO/carbon fiber nanobrushes; XRD patterns of NiO−CoO/carbon fiber precursor (CTB); impedance spectra of NiO/carbon fiber and NiO−CoO/carbon fiber after 200 cycles and clear impedance spectra of the two samples (PDF)

AUTHOR INFORMATION

Corresponding Authors

*E-mail: zhangming@hnu.edu.cn.
*E-mail: lbchen@csu.edu.cn.

Notes

The authors declare no competing financial interest.

ACKNOWLEDGMENTS

This research work has been financially supported by the National Natural Science Foundation of China (21373081, 51404103, 61376073, 51304248), Hunan Provincial Natural Science Foundation of China (14JJ3067), China Postdoctoral Science Foundation (Grants 2013M531800, 2014T70783), Program for Shenghua Overseas Talents from Central South University, and Self-established Project of State Key Laboratory for Power Metallurgy.

REFERENCES

(1) Zhang, Q.; Chen, H.; Wang, J.; Xu, D.; Li, X.; Yang, Y.; Zhang, K. Growth of Hierarchical 3D Mesoporous $NiSi_x/NiCo_2O_4$ Core/Shell Heterostructures on Nickel Foam for Lithium-Ion Batteries. *ChemSusChem* **2014**, *7*, 2325−2334.

(2) Mondal, A. K.; Su, D.; Chen, S.; Kretschmer, K.; Xie, X.; Ahn, H.-J.; Wang, G. A Microwave Synthesis of Mesoporous $NiCo_2O_4$ Nanosheets as Electrode Materials for Lithium-Ion Batteries and Supercapacitors. *ChemPhysChem* **2015**, *16*, 169−175.

DOI: 10.1021/acsami.5b07233
ACS Appl. Mater. Interfaces 2015, 7, 21703−21711

(3) Xu, X.; Dong, B.; Ding, S.; Xiao, C.; Yu, D. Hierarchical $NiCoO_2$ Nanosheets Supported on Amorphous Carbon Nanotubes for High-Capacity Lithium-Ion Batteries with a Long Cycle Life. *J. Mater. Chem. A* **2014**, *2*, 13069−13074.
(4) Zhou, X.; Dai, Z.; Liu, S.; Bao, J.; Guo, Y.-G. Ultra-Uniform SnO_x/Carbon Nanohybrids toward Advanced Lithium-Ion Battery Anodes. *Adv. Mater.* **2014**, *26*, 3943−3949.
(5) Zou, F.; Hu, X.; Li, Z.; Qie, L.; Hu, C.; Zeng, R.; Jiang, Y.; Huang, Y. MOF-Derived Porous $ZnO/ZnFe_2O_4$/C Octahedra with Hollow Interiors for High-Rate Lithium-Ion Batteries. *Adv. Mater.* **2014**, *26*, 6622−6628.
(6) Zhou, G.; Li, F.; Cheng, H.-M. Progress in Flexible Lithium Batteries and Future Prospects. *Energy Environ. Sci.* **2014**, *7*, 1307−1338.
(7) Zheng, G.; Zhang, Q.; Cha, J. J.; Yang, Y.; Li, W.; Seh, Z. W.; Cui, Y. Amphiphilic Surface Modification of Hollow Carbon Nanofibers for Improved Cycle Life of Lithium Sulfur Batteries. *Nano Lett.* **2013**, *13*, 1265−1270.
(8) Liu, B.; Zhang, J.; Wang, X.; Chen, G.; Chen, D.; Zhou, C.; Shen, G. Hierarchical Three-Dimensional $ZnCo_2O_4$ Nanowire Arrays/Carbon Cloth Anodes for a Novel Class of High-Performance Flexible Lithium-Ion Batteries. *Nano Lett.* **2012**, *12*, 3005−3011.
(9) Gao, L.; Qu, F.; Wu, X. Hierarchical WO_3@SnO_2 Core-Shell Nanowire Arrays on Carbon Cloth: a New Class of Anode for High-Performance Lithium-Ion Batteries. *J. Mater. Chem. A* **2014**, *2*, 7367−7372.
(10) Zhou, X.; Wan, L.-J.; Guo, Y.-G. Synthesis of MoS_2 Nanosheet-Graphene Nanosheet Hybrid Materials for Stable Lithium Storage. *Chem. Commun.* **2013**, *49*, 1838−1840.
(11) Song, W.; Hou, X.; Wang, X.; Liu, B.; Chen, D.; Shen, G. Tin Microspheres Grown on Carbon Cloth as Binder-Free Integrated Anode for High Capacity Lithium Storage. *Energy Technol.* **2014**, *2*, 370−375.
(12) Jahel, A.; Ghimbeu, C. M.; Monconduit, L.; Vix-Guterl, C. Confined Ultrasmall SnO_2 Particles in Micro/Mesoporous Carbon as an Extremely Long Cycle-Life Anode Material for Li-Ion Batteries. *Adv. Energy Mater.* **2014**, *4*, 1400025.
(13) Wang, Z.; Luan, D.; Madhavi, S.; Hu, Y.; Lou, X. W. Assembling Carbon-Coated-Fe_2O_3 Hollow Nanohorns on the CNT Backbone for Superior Lithium Storage Capability. *Energy Environ. Sci.* **2012**, *5*, 5252−5256.
(14) Qiao, L.; Wang, X.; Qiao, L.; Sun, X.; Li, X.; Zheng, Y.; He, D. Single Electrospun Porous NiO-ZnO Hybrid Nanofibers as Anode Materials for Advanced Lithium-Ion Batteries. *Nanoscale* **2013**, *5*, 3037−3042.
(15) Xia, Y.; Zhang, W.; Xiao, Z.; Huang, H.; Zeng, H.; Chen, X.; Chen, F.; Gan, Y.; Tao, X. Biotemplated Fabrication of Hierarchically Porous NiO/C Composite from Lotus Pollen Grains for Lithium-Ion Batteries. *J. Mater. Chem.* **2012**, *22*, 9209−9215.
(16) Guan, X.; Nai, J.; Zhang, Y.; Wang, P.; Yang, J.; Zheng, L.; Zhang, J.; Guo, L. CoO Hollow Cube/Reduced Graphene Oxide Composites with Enhanced Lithium Storage Capability. *Chem. Mater.* **2014**, *26*, 5958−5964.
(17) Wang, X.; Qiao, L.; Sun, X.; Li, X.; Hu, D.; Zhang, Q.; He, D. Mesoporous NiO Nanosheet Networks as High Performance Anodes for Li Ion Batteries. *J. Mater. Chem. A* **2013**, *1*, 4173−4176.
(18) Cao, K.; Jiao, L.; Liu, Y.; Liu, H.; Wang, Y.; Yuan, H. Ultra-High Capacity Lithium-Ion Batteries with Hierarchical CoO Nanowire Clusters as Binder Free Electrodes. *Adv. Funct. Mater.* **2015**, *25*, 1082−1089.
(19) Kim, D.-W.; Hwang, I.-S.; Kwon, S. J.; Kang, H.-Y.; Park, K.-S.; Choi, Y.-J.; Choi, K.-J.; Park, J.-G. Highly Conductive Coaxial SnO_2-In_2O_3 Heterostructured Nanowires for Li Ion Battery Electrodes. *Nano Lett.* **2007**, *7*, 3041−3045.
(20) Pan, Q.; Qin, L.; Liu, J.; Wang, H. Flower-Like ZnO-NiO-C Films with High Reversible Capacity and Rate Capability for Lithium-Ion Batteries. *Electrochim. Acta* **2010**, *55*, 5780−5785.
(21) Huang, X. H.; Tu, J. P.; Zhang, B.; Zhang, C. Q.; Li, Y.; Yuan, Y. F.; Wu, H. M. Electrochemical Properties of NiO-Ni Nanocomposite as Anode Material for Lithium Ion Batteries. *J. Power Sources* **2006**, *161*, 541−544.
(22) Xiang, J. Y.; Tu, J. P.; Yuan, Y. F.; Wang, X. L.; Huang, X. H.; Zeng, Z. Y. Electrochemical Investigation on Nanoflower-Like CuO/Ni Composite Film as Anode for Lithium Ion Batteries. *Electrochim. Acta* **2009**, *54*, 1160−1165.
(23) Zhu, X.; Zhu, Y.; Murali, S.; Stoller, M. D.; Ruoff, R. S. Nanostructured Reduced Graphene Oxide/Fe_2O_3 Composite As a High-Performance Anode Material for Lithium Ion Batteries. *ACS Nano* **2011**, *5*, 3333−3338.
(24) Wang, X.; Yang, Z.; Sun, X.; Li, X.; Wang, D.; Wang, P.; He, D. NiO Nanocone Array Electrode with High Capacity and Rate Capability for Li-Ion Batteries. *J. Mater. Chem.* **2011**, *21*, 9988−9990.
(25) Huang, X.-L.; Wang, R.-Z.; Xu, D.; Wang, Z.-L.; Wang, H.-G.; Xu, J.-J.; Wu, Z.; Liu, Q.-C.; Zhang, Y.; Zhang, X.-B. Homogeneous CoO on Graphene for Binder-Free and Ultralong-Life Lithium Ion Batteries. *Adv. Funct. Mater.* **2013**, *23*, 4345−4353.
(26) Mullane, E.; Kennedy, T.; Geaney, H.; Ryan, K. M. A Rapid, Solvent-Free Protocol for the Synthesis of Germanium Nanowire Lithium-Ion Anodes with a Long Cycle Life and High Rate Capability. *ACS Appl. Mater. Interfaces* **2014**, *6*, 18800−18807.
(27) Yoo, E.; Kim, J.; Hosono, E.; Zhou, H.-S.; Kudo, T.; Honma, I. Large Reversible Li Storage of Graphene Nanosheet Families for Use in Rechargeable Lithium Ion Batteries. *Nano Lett.* **2008**, *8*, 2277−2282.
(28) Wang, C.; Wan, W.; Huang, Y.; Chen, J.; Zhou, H. H.; Zhang, X. X. Hierarchical MoS_2 Nanosheet/Active Carbon Fiber Cloth as a Binder-Free and Free-Standing Anode for Lithium-Ion Batteries. *Nanoscale* **2014**, *6*, 5351−5358.
(29) Mo, R.; Lei, Z.; Sun, K.; Rooney, D. Facile Synthesis of Anatase TiO_2 Quantum-Dot/Graphene-Nanosheet Composites with Enhanced Electrochemical Performance for Lithium-Ion Batteries. *Adv. Mater.* **2014**, *26*, 2084−2088.
(30) Yu, Z.-Y.; Chen, L.-F.; Yu, S.-H. Growth of $NiFe_2O_4$ Nanoparticles on Carbon Cloth for High Performance Flexible Supercapacitors. *J. Mater. Chem. A* **2014**, *2*, 10889−10894.
(31) Xiong, Q.-Q.; Tu, J.-P.; Xia, X.-H.; Zhao, X.-Y.; Gu, C.-D.; Wang, X.-L. A Three-Dimensional Hierarchical Fe_2O_3@NiO Core/Shell Nanorod Array on Carbon Cloth: a New Class of Anode for High-Performance Lithium-Ion Batteries. *Nanoscale* **2013**, *5*, 7906−7912.
(32) Masarapu, C.; Subramanian, V.; Zhu, H.; Wei, B. Long-Cycle Electrochemical Behavior of Multiwall Carbon Nanotubes Synthesized on Stainless Steel in Li Ion Batteries. *Adv. Funct. Mater.* **2009**, *19*, 1008−1014.
(33) Ding, S.; Chen, J. S.; Lou, X. W. Glucose-Assisted Growth of MoS_2 Nanosheets on CNT Backbone for Improved Lithium Storage Properties. *Chem. - Eur. J.* **2011**, *17*, 13142−13145.
(34) Qin, J.; He, C.; Zhao, N.; Wang, Z.; Shi, C.; Liu, E.-Z.; Li, J. Graphene Networks Anchored with Sn@Graphene as Lithium Ion Battery Anode. *ACS Nano* **2014**, *8*, 1728−1738.
(35) Zhao, M.-Q.; Zhang, Q.; Huang, J.-Q.; Tian, G.-L.; Nie, J.-Q.; Peng, H.-J.; Wei, F. Unstacked Double-Layer Templated Graphene for High-Rate Lithium-Sulphur Batteries. *Nat. Commun.* **2014**, *5*, 3410.
(36) Banerjee, A.; Bhatnagar, S.; Upadhyay, K. K.; Yadav, P.; Ogale, S. Hollow $Co_{0.85}Se$ Nanowire Array on Carbon Fiber Paper for High Rate Pseudocapacitor. *ACS Appl. Mater. Interfaces* **2014**, *6*, 18844−18852.
(37) Huang, L.; Chen, D.; Ding, Y.; Feng, S.; Wang, Z. L.; Liu, M. Nickel-Cobalt Hydroxide Nanosheets Coated on $NiCo_2O_4$ Nanowires Grown on Carbon Fiber Paper for High-Performance Pseudocapacitors. *Nano Lett.* **2013**, *13*, 3135−3139.
(38) Gong, F.; Wang, H.; Xu, X.; Zhou, G.; Wang, Z.-S. In Situ Growth of $Co_{0.85}Se$ and $Ni_{0.85}Se$ on Conductive Substrates as High-Performance Counter Electrodes for Dye-Sensitized Solar Cells. *J. Am. Chem. Soc.* **2012**, *134*, 10953−10958.
(39) Wang, Y. F.; Zhang, L. J. Simple Synthesis of CoO-NiO-C Anode Materials for Lithium-Ion Batteries and Investigation on Its Electrochemical Performance. *J. Power Sources* **2012**, *209*, 20−29.

DOI: 10.1021/acsami.5b07233
ACS Appl. Mater. Interfaces 2015, 7, 21703−21711

(40) Chan, C. K.; Peng, H.; Liu, G.; et al. High-Performance Lithium Battery Anodes Using Silicon Nanowires. *Nat. Nanotechnol.* **2008**, *3*, 31−35.
(41) Lei, D.; Zhang, M.; Qu, B.; Chen, L.; Wang, Y.; Zhang, E.; Xu, Z.; Li, Q.; Wang, T. α-Fe_2O_3 Nanowall Arrays: Hydrothermal Preparation, Growth Mechanism and Excellent Rate Performances for Lithium Ion Batteries. *Nanoscale* **2012**, *4*, 3422−3426.
(42) Guan, B.; Guo, D.; Hu, L.; Zhang, G.; Fu, T.; Ren, W.; Li, J.; Li, Q. Facile Synthesis of $ZnCo_2O_4$ Nanowire Cluster Arrays on Ni Foam for High-Performance Ssymmetric Supercapacitors. *J. Mater. Chem. A* **2014**, *2*, 16116−16123.
(43) Ji, M.; Wang, C.; Bai, Y.; Yu, M.; Wang, Y. Structural Evolution of Polyacrylonitrile Precursor Fibers during Preoxidation and Carbonization. *Polym. Bull.* **2007**, *59*, 527−536.
(44) Yuan, C.; Li, J.; Hou, L.; Zhang, X.; Shen, L.; Lou, X. W. Ultrathin Mesoporous $NiCo_2O_4$ Nanosheets Supported on Ni Foam as Advanced Electrodes for Supercapacitors. *Adv. Funct. Mater.* **2012**, *22*, 4592−4597.
(45) Cao, L.; Wang, D.; Wang, R. NiO Thin Films Grown Directly on Cu Foils by Pulsed Laser Deposition as Anode Materials for Lithium Ion Batteries. *Mater. Lett.* **2014**, *132*, 357−360.
(46) Tan, Z. a.; Zhang, W.; Qian, D.; Cui, C.; Xu, Q.; Li, L.; Li, S.; Li, Y. Solution-Processed Nickel Acetate as Hole Collection Layer for Polymer Solar Cells. *Phys. Chem. Chem. Phys.* **2012**, *14*, 14217−14223.
(47) Varghese, B.; Reddy, M. V.; Yanwu, Z.; Lit, C. S.; Hoong, T. C.; Subba Rao, G. V.; Chowdari, B. V. R.; Wee, A. T. S.; Lim, C. T.; Sow, C.-H. Fabrication of NiO Nanowall Electrodes for High Performance Lithium Ion Battery. *Chem. Mater.* **2008**, *20*, 3360−3367.
(48) An, C.; Wang, Y.; Huang, Y.; Xu, Y.; Jiao, L.; Yuan, H. Porous $NiCo_2O_4$ Nanostructures for High Performance Supercapacitors via a Microemulsion Technique. *Nano Energy* **2014**, *10*, 125−134.
(49) Du, Y.; Zhu, X.; Zhou, X.; Hu, L.; Dai, Z.; Bao, J. Co_3S_4 Porous Nanosheets Embedded in Graphene Sheets as High-Performance Anode Materials for Lithium and Sodium Storage. *J. Mater. Chem. A* **2015**, *3*, 6787−6791.
(50) Zhang, M.; Uchaker, E.; Hu, S.; Zhang, Q.; Wang, T.; Cao, G.; Li, J. CoO-Carbon Nanofiber Networks Prepared by Electrospinning as Binder-Free Anode Materials for Lithium-Ion Batteries with Enhanced Properties. *Nanoscale* **2013**, *5*, 12342−12349.
(51) Zhu, X. J.; Guo, Z. P.; Zhang, P.; Du, G. D.; Zeng, R.; Chen, Z. X.; Li, S.; Liu, H. K. Highly Porous Reticular Tin-Cobalt Oxide Composite Thin Film Anodes for Lithium Ion Batteries. *J. Mater. Chem.* **2009**, *19*, 8360−8365.
(52) Tang, Q.; Chen, M.; Wang, L.; Wang, G. A Novel Asymmetric Supercapacitors Based on Binder-free Carbon Fiber Paper@Nickel Cobaltite Nanowires and Graphene Foam Electrodes. *J. Power Sources* **2015**, *273*, 654−662.
(53) Huang, X. H.; Tu, J. P.; Zhang, C. Q.; Zhou, F. Hollow Microspheres of NiO as Anode Materials for Lithium-Ion Batteries. *Electrochim. Acta* **2010**, *55*, 8981−8985.
(54) Choi, S. H.; Kang, Y. C. Ultrafast Synthesis of Yolk-Shell and Cubic NiO Nanopowders and Application in Lithium Ion Batteries. *ACS Appl. Mater. Interfaces* **2014**, *6*, 2312−2316.
(55) Mondal, A. K.; Su, D.; Chen, S.; Xie, X.; Wang, G. Highly Porous $NiCo_2O_4$ Nanoflakes and Nanobelts as Anode Materials for Lithium-Ion Batteries with Excellent Rate Capability. *ACS Appl. Mater. Interfaces* **2014**, *6*, 14827−14835.
(56) Guo, D.; Luo, Y.; Yu, X.; Li, Q.; Wang, T. High Performance $NiMoO_4$ Nanowires Supported on Carbon Cloth as Advanced Electrodes for Symmetric Supercapacitors. *Nano Energy* **2014**, *8*, 174−182.
(57) Mai, Y. J.; Tu, J. P.; Xia, X. H.; Gu, C. D.; Wang, X. L. Co-Doped NiO Nanoflake Arrays toward Superior Anode Materials for Lithium Ion Batteries. *J. Power Sources* **2011**, *196*, 6388−6393.
(58) Huang, X. H.; Yuan, Y. F.; Wang, Z.; Zhang, S. Y.; Zhou, F. Electrochemical Properties of NiO/Co-P Nanocomposite as Anode Materials for Lithium Ion Batteries. *J. Alloys Compd.* **2011**, *509*, 3425−3429.
(59) Liu, L.; Li, Y.; Yuan, S.; Ge, M.; Ren, M.; Sun, C.; Zhou, Z. Nanosheet-Based NiO Microspheres: Controlled Solvothermal Synthesis and Lithium Storage Performances. *J. Phys. Chem. C* **2010**, *114*, 251−255.
(60) Hassan, M. F.; Rahman, M. M.; Guo, Z.; Chen, Z.; Liu, H. SnO_2-NiO-C Nanocomposite as a High Capacity Anode Material for Lithium-Ion Batteries. *J. Mater. Chem.* **2010**, *20*, 9707−9712.

DOI: 10.1021/acsami.5b07233
ACS Appl. Mater. Interfaces 2015, 7, 21703−21711